



CHAPTER IV
SYNTHESIS AND CHARACTERIZATION OF SIZE-CONTROLLED
HEMATITE (α -Fe₂O₃) NANOPARTICLES VIA THE CHEMICAL
PRECIPITATION METHOD

Kitibodee Supattarasakda¹, Karat Petcharoen¹, Tharaporn Pernpool¹,
Anuvat Sirivat^{1,2,*}, and Wanchai Lerdwijitjarud³

¹ The Petroleum and Petrochemical College, Chulalongkorn University, Bangkok,
10330, Thailand

² Center of Excellence on Petrochemical and Materials Technology, Bangkok, 10330,
Thailand

³ Department of Materials Science and Engineering, Faculty of Engineering and In-
dustrial Technology, Silpakorn University, Nakhon Pathom, 73000, Thailand

* Corresponding author

E-mail: anuvat.s@chula.ac.th; Tel: 662 218 4131; Fax: 662 611 7221

4.1 Abstract

Hematite ($\alpha\text{-Fe}_2\text{O}_3$) nanoparticles were synthesized from the ferrihydrite precursor via a simple chemical precipitation method by using sodium hydroxide as a precipitating agent, with trace amounts of Fe(II) as a catalyst, and under nitrogen atmosphere. The structure and morphology of the synthesized hematite particles were characterized by XRD, FT-IR, TG/DTA, and FE-SEM. Moreover, the electrical and magnetic properties were studied by using an electrometer and a vibrating sample magnetometer (VSM), respectively. The results indicated that the synthesized products were of a single phase of the hexagonal structure hematite without any other impurities. The physical morphology of the synthesized hematite appeared to be composed of a large number of very small particles which can be called as the “raspberry shape”. The particle size of the synthesized hematite could be successfully controlled to be in the range of 50-150 nm possessing three different morphologies, consisting of the spherical-like, the cubic-like, and the ellipsoidal shape by adjusting the synthesis conditions. The smallest particle possessed the highest electrical conductivity of 5.2×10^{-3} S/cm which was higher than that of the largest particle by about 5.4 times. On the other hand, the largest particle exhibited weak ferromagnetism had the highest saturation magnetization (M_s) of 1.94 emu/g which was higher than that of the smaller particle changed to behave the superparamagnetism. Furthermore, the different particle shapes which were shown to critically affect the electrical and magnetic properties of the products were also discussed.

Keywords: Size-controlled hematite ($\alpha\text{-Fe}_2\text{O}_3$); Magnetic nanoparticles; Chemical precipitation method; Electrical conductivity; Superparamagnetic behavior

4.2 Introduction

Magnetic nanoparticles can exhibit many unique properties such as chemical, electrical, and magnetic properties which are advantageous for using in a variety of the applications. There are many types of magnetic particles, and one of the most important groups is iron oxides generally existed in forms of hematite (α -Fe₂O₃), magnetite (Fe₃O₄) and maghemite (γ -Fe₂O₃), which are utilized for the different specific applications (Teja and Koh 2009). Hematite (α -Fe₂O₃), which is the most stable iron oxide under the ambient conditions, has an increasing interest in the fields of nanoscience and nanotechnology because of its potential applications in inorganic pigments (Cornell and Schwertmann 1996), catalysts (Brown *et al.* 1998), gas and humidity sensors (Chauhan *et al.* 1999; Huo *et al.* 2000), photoanode for photoelectrochemical cells (Watanabe and Kozuka, 2003), photoelectrolysis reactors (Kay *et al.* 2006), water treatment (Cao and Zhu 2008), and lithium ion batteries (Wu *et al.* 2008).

The preparation method is a key factor in determining the particle size, the morphology, the particle size distribution, the surface chemistry and therefore the properties of the final products. Up to now, a variety of methods have been reported in the literatures on the preparation of hematite nanoparticles, such as the hydrolysis method (Raming *et al.* 2002; Music *et al.* 2003), the hydrothermal treatment (Lian *et al.* 2004; Zhang *et al.* 2008; Sun *et al.* 2010), the chemical precipitation method (Liu *et al.* 2005, 2007), the solvothermal process (Lu *et al.* 2006), the facile solution route (Min *et al.* 2007), the microemulsion method (Bumajdad *et al.* 2007; Han *et al.* 2011), and etc. In comparison of all methods, the chemical precipitation method is probably the simplest and the most effective as well as of a relatively low cost without requirement of the special equipment or any additives. Recently, a simple chemical precipitation system via the catalytic phase transformation process has been successfully employed to synthesize hematite (α -Fe₂O₃) nanoparticles (Liu *et al.* 2007). The experimental results have revealed that this method has several advantages, such as can use a high reactant concentration, require a very short reaction time as well as a low reaction temperature, and get a high purity products of hematite nanoparticles.

Controlling of the particle size and morphology is considerably important in the preparation of hematite nanoparticles, because properties and applications of the ultrafine particles depend drastically on the particle size, morphology and monodispersibility of the products (Diamandescu *et al.* 1999). Until now, several researches have been focused on the study of the factors affecting the particle size and shape of the synthesized hematite nanoparticles. Those parameters have been reported in the literatures, such as the reactant concentration, the solution pH, the reaction time and temperature, the ionic strength, the anions, the surfactant, and the nature of iron salts (Cornell and Giovanoli 1985; Schwertmann *et al.* 1999; Lu *et al.* 2006; Liu *et al.* 2007; Min *et al.* 2007; Zhang *et al.* 2008; Kandori *et al.* 2008; Sun *et al.* 2010). However, in some cases such as using the surfactants or anions, the additional steps of removal the excess amount of chemicals used are required and the products obtained may have the lower properties compared to using the simple method.

In this work, a simple chemical precipitation method has been employed to directly synthesize hematite (α -Fe₂O₃) nanoparticles, with trace amounts of Fe(II) as a catalyst, under nitrogen atmosphere. The influences of the synthesis conditions, consisting of the precursor concentration (C), the solution pH, the amount of catalyst ($n_{\text{Fe(II)}}/n_{\text{Fe(III)}}$), the ionic strength (I), the reaction temperature and the reaction time on particle size and morphology of the synthesized hematite have been systematically investigated. Moreover, the electrical conductivity and magnetic properties depending on the particle size and shape of the synthesized hematite are also reported here

4.3 Experimental

4.3.1 Chemicals

All chemicals used in this work were analytical reagent grade from the commercial market and used without further purification. In this synthesis method, ferric chloride anhydrous (FeCl₃; Ajax Finechem, 98.0%) was used as the reactant, ferrous chloride tetrahydrate (FeCl₂·4H₂O; Sigma Aldrich, 99.0%) was used as the catalyst, sodium hydroxide (NaOH; Lobal Chemie, 98.0%) and ammonium hydroxide (NH₄OH; Merck, 25.0 % NH₃ in water) were used as the precipitating agents, sodium chloride (NaCl; Lab-Scan, 99.0%) was used to control the ionic strength (I)

of the solution, and distilled water was used as the reaction medium and used to remove the sodium chloride from the product.

4.3.2 Synthesis of Hematite Nanoparticles

Hematite nanoparticles were synthesized via the chemical precipitation method as described by Liu *et al.* (2007) with some alterations. In a typical preparation, NaOH solution (6.0 M, 25 ml) was added into Fe(III) solution (1.0 M, 50 ml) until reached pH 7 under the condition of vigorous stirring at room temperature. In this mixed system, the brown precipitates precursor (Fe(OH)₃) formed were confirmed to be 2-line ferrihydrite by using XRD. The agitation was continued for an additional 10 min, followed by adding trace amounts of Fe(II) ions ($n_{\text{Fe(II)}}/n_{\text{Fe(III)}} = 0.02$) into the system. The pH of the system was readjusted to the desired pH 7 once again with a dilute NaOH solution (1.0 M) and at the same time the total volume of each system was adjusted to 100 ml so that the total concentration (C) of the precursor reached 0.5 M. The suspension was heated to a boiling point and kept refluxing for 1h under vigorous stirring. All stages of the experiment were carried out under pure N₂ gas to avoid the oxidation of Fe(II). The final product was filtered off, washed thoroughly with distilled water, and then dried at about 70-80 °C. In addition, the preparation conditions were adjusted to study various effects while holding the other parameters constant.

4.3.3 Characterization of Hematite Nanoparticles

A powder X-ray diffractometer (Bruker AXS, D8 Advance) was used to examine the crystal structure of the synthesized hematite particles which were below the nanometer scale. The Cu K α ($\lambda = 1.5406 \text{ \AA}$) radiation source was operated at 40 kV/30 mA and used the K β filter to eliminate the interference peak. The experiments were recorded by monitoring the diffraction appeared in the diffraction angle (2θ) range from 10.00 to 80.00 deg with scan speed of 1.00 deg/min and scan step of 0.02 deg.

A Fourier transform infrared spectrometer (Thermo Nicolet, Nexus 670), with a deuterated triglycine sulfate detector, was used to characterize the functional groups of the synthesized hematite particles. The sample powder was

grounded in a mortar and mixed with dried KBr at ratio of sample:KBr was about 1:20, then the mixed powder was compressed into the pellets under the pressure of 7 tons. The absorption mode was run 64 scans with a resolution of $\pm 4 \text{ cm}^{-1}$ in the wavenumber in range of 4000-400 cm^{-1} .

A thermogravimetric/differential thermal analyzer (Perkin Elmer, Pyris Diamond) was used to determine the thermal behavior of the synthesized hematite particles. The experiment was carried out by weighting a powder sample of 1-5 mg and loaded into a platinum pan. The mass change under the temperature scan from 30 to 600 °C at a heating rate of 10 °C/min and under the nitrogen flow was monitored and recorded.

A field-emission scanning electron microscope (Hitachi, S-4800) was used to examine the morphological structure and to determine the particle size of the synthesized hematite particles. The sample powder was placed on the holder with an adhesive tape and coated with a thin layer of platinum using an ion sputtering device (Hitachi, E-1010) for 100 sec prior to observation under FE-SEM. The scanning electron images were investigated by using an acceleration voltage of 5.0 kV with a magnification in the range of 50.0-200k times. The particle size and particle size distribution of the synthesized hematite particles were determined by the professional image processing and analysis software of SemAfore over 2-3 FE-SEM images by the quantitative statistical method.

A surface area analyzer (Thermo finnigan, Sorptomatic 1990) was used to measure the specific surface area of the synthesized hematite particles. The absorbent sample was weighed and outgassed at 300 °C for 12 h under vacuum to eliminate volatile adsorbate on the surface. The data were obtained by adsorption and desorption of He and N₂ gases, respectively. The BET surface area was determined by using the static volumetric method.

An electrometer (Keithley, 6517A), with a custom-built two-point probe, was used to measure the electrical conductivity which is the inversion of the specific resistivity (ρ) that indicates the ability of material to transport electrical charge. The meter consisted of a probe making contact on a surface of the sample in a disc shape. The applied voltage was plotted versus the resultant current to determine the linear Ohmic regime of each sample based on the Van der Pauw method.

The applied voltage and the current in the linear Ohmic regime were converted to the electrical conductivity of the samples using equation (1) as follow:

$$\sigma = \frac{1}{\rho} = \frac{1}{R_s \times t} = \frac{I}{K \times V \times t} \quad (4.1)$$

where σ is the specific conductivity (S/cm), ρ is the specific resistivity ($\Omega \cdot \text{cm}$), R_s is the sheet resistivity (Ω), I is the resultant current (A), K is the geometric correction factor (7.36×10^{-4}) which is calibrated by using the standard silicon wafer, V is the applied voltage (V), and t is the thickness of the disc sample (cm).

A vibrating sample magnetometer (LakeShore, 7404), with a 4-inch electromagnet, was used to study the magnetic properties of the synthesized hematite particles. The magnetization curves were measured under the maximum magnetic field strength of 8000.0 Oe at room temperature to determine the hysteresis loops. The data were taken with a scan speed of 10 sec/point to complete the 280 points of the hysteresis loop.

4.4 Results and Discussion

4.4.1 Characterization of the Synthesized Hematite Nanoparticles

The purity and crystallinity of the precursor and the synthesized products were examined by using powder XRD measurement, as shown in Figure 4.1. It can be seen that the precursor exhibits two extremely broad peaks at 2θ about 36.0° and 62.5° which can be attributed to the poorly crystalline phase of 2-line ferrihydrite (Cornell and Schwertmann 2003). This poorly ordered compound is metastable which can be further transformed to hematite at the appropriate physico-chemical conditions. From the XRD pattern of the synthesized product, it is evident that all of the peaks can be indexed to the hexagonal structure of hematite (space group: $R\bar{3}c$), with lattice constants of $a = 0.5034 \text{ nm}$ and $c = 1.375 \text{ nm}$ (Teja and Koh 2009), which are in good agreement with the literature result (JCPDS Card No. 33-0664). The narrow sharp peaks indicate that the hematite products are highly crystalline (Su

et al. 2011); implying that the high purity of the synthesized hematite particles is obtained by using this synthesis method.

The functional groups of the ferrihydrite precursor and the synthesized hematite particles were characterized by using FT-IR measurement, as shown in Figure 4.2. From the FT-IR spectrum of the ferrihydrite precursor, the very broad band centered at 3384 cm^{-1} and peak at 1622 cm^{-1} are observed and can be attributed to the superposition of stretching vibrations of hydroxyl (OH) groups and water molecules. The strong and board band with peaks at 431 and 578 cm^{-1} are typical for the low crystalline ferrihydrite (Ristic *et al.* 2007). For the result of the hematite product, the strong absorption peaks at 475 and 560 cm^{-1} are attributed to the Fe–O bond vibrations which are in accordance with those observed for hematite particles (Jing and Wu 2004; Liu *et al.* 2007). The very broad absorption band centered at 3449 and peak at 1632 cm^{-1} are assigned to the stretching and bending vibrations of hydroxyl (OH) groups and/or water molecules, respectively. This result indicates the presence of a small amount of adsorbed water on the surface of the product and the structural hydroxyl groups in the product as the products are prepared in the aqueous solution. Both XRD and FT-IR results indicate that no any other by-products are present in the synthesized products.

The thermal behavior of the synthesized hematite particles were determined by using TG/DTA measurement, as shown in Figure 4.3. The synthesized hematite particles exhibit an endothermic DTA peak (*dashed line* in Figure 4.3) at $25\text{-}50\text{ }^{\circ}\text{C}$ due to the elimination of adsorbed water on the surface of the product (Kandori *et al.* 2008). The TG curve (*solid line* in Figure 4.3) of the hematite particles shows two weight loss steps from room temperature to $600\text{ }^{\circ}\text{C}$. The mass loss of ca. 4.0% continues slowly up to $200\text{ }^{\circ}\text{C}$ which can be attributed to the removal of adsorbed water on the surface, and one more small mass loss (ca. 0.5%) can be recognized at $200\text{-}400\text{ }^{\circ}\text{C}$. This latter mass loss is assigned to the elimination of hydroxyl ions (OH⁻) included in hematite crystal structure (Lu *et al.* 2006). These results are consistent with the FT-IR result of the synthesized hematite which indicates the presence of adsorbed water and hydroxyl surface structure. Furthermore, the hydroxyl (OH) surface structure of the synthesized hematite is very sensitive to the moisture

molecules; therefore, it is appropriate to use it as the humidity sensor material (Chauhan *et al.* 1999).

4.4.2 Particle Sizes of the Synthesized Hematite Nanoparticles

The average particle sizes of the synthesized hematite particles under the effect of various preparation conditions are shown in Figure 4.4. For the effect of the precursor concentration (Figure 4.4 (a)), the average particle diameter of hematite decreases from 139.5 nm to 49.3 nm (factor of 2.8) when decreasing the precursor concentration from 0.5 M to 0.1 M. The reason is that the nucleation of hematite takes place within the ferrihydrite precursor aggregate and the amount of Fe in the aggregate determines the final size of the hematite particles; therefore, it is related to the aggregate size of the precursor (Schwertmann *et al.* 1999). However, the precursor concentration cannot further decrease because a low concentration of precursor (e.g., $C = 0.05$ M) needs a very long time to reach the saturation concentration to form hematite particles (Schwertmann and Cornell 2000) and also gets a very low yield percentage about 36 % compared to 61 % of hematite with using $C = 0.1$ M.

In order to study the effect of solution pH, the precursor concentration $C = 0.3$ M which possessed the moderate particle size was chosen to use in our further study. The effect of the solution pH on the particle size of the products was studied when other preparation conditions were held constant. Figure 4.4 (b) shows that the average particle size of the products increases as the solution pHs increases from pH 5 until reaching the pH 7, and then the particle size decreases as the solution pH further increases up to pH 9 which is consistent with the result of Liu *et al.* (2007). This can be explained by the different species of Fe(II) ions formed at the different pH; in the pH range from 5 to 9, Fe(II) ions exist in the form of Fe^{2+} , FeOH^+ , $\text{Fe}(\text{OH})_2$, and $\text{Fe}(\text{OH})_3^-$. The predominated species of Fe(II) ions at pH 7 (FeOH^+) and at pH 9 ($\text{Fe}(\text{OH})_2$) are proposed to catalyze the dissolution/precipitation mechanism (growth step) and the solid-state transformation (nucleation step), respectively (Liu *et al.* 2005). Therefore, at pH 7 the crystal growth rate is very high results in the larger particle size; while at pH 9, the nucleation is predominant leads to the smaller particle size.

The effect of the amount of Fe(II) using as a catalyst was investigated as shown in Figure 4.4 (c). In the presence of Fe(II), not only the solid-state transformation (nucleation step) from ferrihydrite is accelerated, but the dissolution of ferrihydrite is also accelerated, leading to the rapid formation of hematite through the dissolution/reprecipitation mechanism (growth step) (Liu *et al.* 2005). In this part, the solution pH was controlled at pH 7 to study the effect of Fe(II) in the crystal growth step of the phase transformation process. The result clearly demonstrates that the average particle size of hematite decreases from 134.5 nm to 83.1 nm (about 1.6 times) with decreasing the molar ratio of Fe(II) to Fe(III) ($n_{\text{Fe(II)}}/n_{\text{Fe(III)}}$) from 0.05 to 0.01, because Fe(II) acts as a catalyst for the phase transformation from 2-line ferrihydrite to hematite; so the lower the amount Fe(II) used, the smaller the particle size of hematite is obtained.

The effect of the ionic strength on the particle size of hematite was carried out by adding a certain amounts of NaCl solution (5.0 M) into the suspension to control the ionic strength of the solution in the range of 1.0 to 2.0. Based on the literature data, the high ionic strength can lower the aggregation and retard the dissolution of the ferrihydrite precursor (Cornell and Giovanoli 1985). However, our result as shown in Figure 4.4 (d) demonstrates that there is no significant effect of ionic strength on the particle size of hematite in the range of ionic strength values used in the present preparation. This may explain the finding that the rapid growth rate of hematite particles as catalyzed by Fe(II) may overcome the effect of the ionic strength.

The effects of the reaction temperature and reaction time on the particle size of the products were also studied in the range of 60-100 °C and 10-120 min which are the appropriate conditions to synthesize the hematite. These results also show that the reaction temperature and reaction time do not significantly affect the particle size of the synthesized hematite. However, according to the literature data (Liu *et al.* 2010), the reaction temperature and the reaction time are very important to the transformation process from ferrihydrite to various iron (hydr)oxides, such as lepidocrocite (γ -FeOOH), goethite (α -FeOOH), magnetite (Fe_3O_4), and also hematite (α - Fe_2O_3).

4.4.3 Particle Morphologies of the Synthesized Hematite Nanoparticles

The spherical-like hematite nanoparticles are successfully prepared by using a typical synthesis condition, as shown in the Figure 4.5. The FE-SEM image in Figure 4.5 (a) shows the morphology of the ferrihydrite precursor which is of a very small sphere with the average diameter of 11.5 nm. The synthesized hematite particles prepared by varying the initial precursor concentrations are shown in Figure 4.5 (b-d). It can be clearly seen that the lower the precursor concentration used, the smaller the particle size of hematite is obtained. The average sizes of the hematite particles are about 50-140 nm, which are higher than that of the particle sizes obtained by Liu *et al.* (2007). However, the ferrihydrite precursor and hematite particles prepared have a normal size distribution as shown in the *inset plots* of Figure 4.5 (a-d).

The synthesized hematite particles with the different morphologies are also successfully prepared, as shown in Figure 4.6. The spherical-like (Figure 4.6 (a, b)), the cubic-like (Figure 4.6 (c)), and the ellipsoidal hematite particles (Figure 4.6 (d)) can be obtained by preparing with Fe(II), with very small amount of Fe(II) ($n_{\text{Fe(II)}}/n_{\text{Fe(III)}} = 0.001$), and with NH_4OH instead of NaOH that using in a typical synthesis, respectively. This result can be explained by the difference of the formation mechanism occurred. In a typical synthesis condition, the hematite particles are proposed to form through the “nucleation-aggregation-dissolution-recrystallization-Oswald ripening” mechanism; while in the system with a very small amount of Fe(II) used, the products are proposed to form via the “nucleation-aggregation-recrystallization-Oswald ripening” mechanism as described by Lian *et al.* (2009). For the ellipsoidal particles, the formation may be occurred via the anisotropic growth mechanism by the adsorption of ions on the surface planes parallel to the basal [001] plane of the hematite nuclei (Hu and Yu 2008). This can prevent the growth of hematite in those directions and allow only the recrystallization along the c-axis which produces the final ellipsoidal particles (Ocana *et al.* 1995). The high magnification FE-SEM image of hematite particles clearly reveals that the surfaces of hematite particles are not smooth (Figure 4.6 (b)). The whole hematite particle seems to be composed of a large number of small nanoparticles of ferrihydrite precursor (*inset* of Figure 4.6 (b)) which can be called as the “raspberry shape” (Han and Armes 2003).

Moreover, this special surface structure of the product leads to a bigger specific surface area compared to the smooth surface particle, which is the favored property for using in catalyst and gas sensor applications (Brown *et al.* 1998; Huo *et al.* 2000). In comparison, the specific surface area of our smallest hematite particles (average diameter of 49.3 nm) is 55.4 m²/g which is higher than that of the value reported by Liu *et al.* (2007) that was 31.83 m²/g for the particle size about 60-80 nm.

4.4.4 Electrical Conductivity of the Synthesized Hematite Nanoparticles

The specific conductivities (σ) of the synthesized hematite particles with different particle sizes and shapes were measured by using electrical conductivity measurement, as shown in Figure 4.7. The smallest hematite particles possess the highest electrical conductivity of 5.2×10^{-3} S/cm which is in the range of the semi-conducting materials (σ is about 10^3 - 10^{-8} S/cm). On comparing with our previous work (Petcharoen and Sirivat 2012), the specific conductivity of the hematite particles is higher than that of the highest value of the magnetite particles (1.3×10^{-3} S/cm) about 4 times. In addition, the result shows that the particle size of hematite critically affects to their electrical conductivity which increases about 5.4 times with decreasing particle size from about 140 nm to 50 nm. The reason is the smaller particles provide the tight aggregation of particles results in the better packing efficiency of the smaller particles; therefore, more contact area for electron transfer between particles is obtained (Chunhui *et al.* 2008). Another reason is based on the adsorption of water on the surface of hematite and then the water molecules react reversibly with the lattice iron (Fe) to produce free electron leading to the increase in the electrical conductivity. Consequently, the decrease in the particle size leads to more surface area thus providing more active iron sites available for adsorbing water (Chauhan *et al.* 1999). The latter reason is confirmed by the specific surface area measurement which is found that the specific surface area increases from 18.5 m²/g to 55.4 m²/g (factor of 3.0), when the particle size decreases from about 140 nm to 50 nm. For hematite particles with different in size and shape, the cubic-like particles (130 nm; *square* in Figure 4.7) have the specific conductivity value about 1.0×10^{-3} S/cm which closes to the value of the largest spherical-like particles (9.7×10^{-4} S/cm), but the ellipsoidal particles (120 nm; *triangle* in Figure 4.7) have a lower

conductivity value about 3.2×10^{-4} S/cm because the ellipsoidal particles are more difficult to pack together comparing to the spherical-like particles.

4.4.5 Magnetic Properties of the Synthesized Hematite Nanoparticles

The magnetic properties of the synthesized hematite particles were studied by using a VSM measurement at room temperature. The magnetization curves of the synthesized hematite particles with different particle sizes and different morphologies are shown in Figure 4.8 (a) and (b), respectively.

It is clearly seen that the largest hematite particle (*dashed line* in Figure 4.8 (a)) exhibits a large hysteresis loop, and the hysteresis loop decreases with decreasing of the particle size (*dotted line* in Figure 4.8 (a)). The smallest hematite particle (*solid line* in Figure 4.8 (a)) has almost no remnant magnetization (M_r) at zero magnetic field strength and has a very low coercive force (H_c) (*inset plot* of Figure 4.8 (a)), which is an indication of the superparamagnetism. According to the literature, when the size of the magnetic particles decreases, the particles change from a multidomain to a single domain because the formation of domain walls becomes energetically unfavorable (Vatta *et al.* 2006). If the single domain particles become small enough, the magnetic moments in the domain fluctuates in direction because of thermal agitation, which leads to the superparamagnetism (Zhang *et al.* 2008). The smallest hematite particles obtained (49.3 nm) are apparently single-domain particles, which also exhibit superparamagnetism. This implies that the magnetic domain size of these particles is approximately 50 nm, which is in agreement with the largest size of 41 nm as reported by Raming *et al.* (2002). The magnetic parameters consisting of H_c , M_r , M_s , and M_r/M_s of the synthesized hematite particles with different particle sizes are summarized in Table 4.1, where H_c is the coercive force; M_r is the remanence magnetization (at $H = 0$ Oe); and M_s is the saturation (maximum) magnetization. The H_c and M_r/M_s values are both measured for the amount of ferromagnetic behavior presents in the samples. It is clearly seen that the ferromagnetic nature decreases with the particle size (Figure 4.8 (a) and Table 4.1), because the anisotropic energy barrier for rotation of magnetic moments is proportional to the particle volume (Raming *et al.* 2002). It is noted that the saturation magnetization (M_s) also decreases from 1.94 emu/g to 0.80 emu/g with decreasing of particle size from

140 nm to 50 nm because of the increase in surface to volume ratio of the smaller particles. This can result in the higher disordered spin configuration leading to the reduction of the net magnetic moment of the hematite particles which is known as the surface effect (Huang *et al.* 2003; Zysler *et al.* 2004; Sun *et al.* 2010).

The magnetic hysteresis loops were obtained for all samples (particle sizes are about 120-140 nm) of different morphologies, as shown in Figure 4.8 (b). The hysteresis loops reveal that the resultant hematite nanostructures are weak ferromagnetic at room temperature. It can be seen that there are some differences among these three samples. The magnetic parameters consisting of H_c , M_r , M_s , and M_r/M_s of the synthesized hematite particles with different morphologies are also summarized in Table 4.1. Generally, the magnetization of ferromagnetic materials is very sensitive to the microstructure of a particular sample; therefore, the difference in the remanence magnetization (M_r) for the samples is related to the particle morphology and the magnitude of coercive force (H_c) is proportional to the particle size (Cao *et al.* 1997; Li *et al.* 2000). In fact, the hematite particles prepared in various preparation conditions are both different in morphology and particle size, as showed in FE-SEM images (Figure 4.6). In addition, the particle size of the spherical-like hematite is about 140 nm and that of the cubic-like and ellipsoidal hematite are about 130 and 120 nm, respectively. As can be seen from Table 4.1, the saturation magnetization (M_s) value of the spherical-like particles (1.94 emu/g) is higher than that of the cubic-like particles (1.78 emu/g), and the ellipsoidal particles (1.63 emu/g), which may be attributed to the increase in surface effect with decreasing particle size as described previously. It is suggested that the higher M_r and H_c of the ellipsoidal hematite compared to the cubic-like hematite (*inset plot* of Figure 4.8 (b) and Table 4.1) may be associated with their higher aspect ratio, because the shape anisotropy can prevent the magnetization except along the easy magnetic axes result in more difficult magnetization and demagnetization (Tang *et al.* 2006). This shape anisotropy critically influences the magnetic properties, such as lower the saturation magnetization (M_s), as well as increase the remanence magnetization (M_r) and coercive force (H_c) (Liu *et al.* 2005; Wang *et al.* 2005). In comparison, our hematite particles have a moderate M_s value comparing to that of the value reported in the literatures using the other methods which are in the range from low value as 0.03 emu/g (Zhang *et al.* 2008) to

high value as 5.1 emu/g (Sarangi *et al.* 2009). This may be explained by the fact that the different synthesis methods usually provide the different particle sizes, morphologies and also surface structures which critically affect to the magnetic properties of the products as already discussed.

4.5 Conclusions

The synthesized particles fabricated at pH 5-9 and at temperatures between 60-100 °C for 1h are confirmed to be the single phase hexagonal structure and highly crystalline hematite. The physical morphology of the synthesized hematite seems to be composed of a large number of very small particles with the highest specific surface area of 55.4 m²/g and consisting of the hydroxyl (OH) surface structure. The particle size of the synthesized hematite decreases with decreasing of the precursor concentration and the amount of catalyst. The solution pH provides the maximum particle size at the neutral pH, which is preferred for the growth step by dissolution/reprecipitation process. The effect of the transformation mechanism from ferrihydrite to hematite can overcome the effect of the ionic strength of the reaction system. The reaction temperature and the reaction time have no significant effect on the hematite particle size. The synthesized hematite particles can be successfully controlled to be in the range of 50-150 nm possessing three different morphologies, consisting of the spherical-like, the cubic-like, and the ellipsoidal shapes. The particle size and shape of the synthesized hematite critically affect their electrical and magnetic properties. The specific conductivity (σ) increases with decreasing of the hematite particle size and the smallest particle possesses the highest conductivity of 5.2×10^{-3} S/cm. The large hematite particles exhibit hysteresis loops indicated the weak ferromagnetic behavior at room temperature with the highest M_s of 1.94 emu/g, and change from multidomain to single domain exhibited the superparamagnetism as the particle size further decreases. Moreover, the different shape hematite also shows varying magnitudes of the magnetic parameters in the hysteresis loops as discussed.

4.6 Acknowledgements

The authors are grateful for the financial supports from the Petroleum and Petrochemical College, the Center of Excellence on Petrochemical, and Materials Technology, the Conductive and Electroactive Polymers Research Unit of Chulalongkorn University, the Thailand Research Fund (TRF-BRG), and the Royal Thai Government

4.7 References

- Brown ASC, Hargreaves JSJ, Rijniersce B (1998) A study of the structural and catalytic effects of sulfation on iron oxide catalysts prepared from goethite and ferrihydrite precursors for methane oxidation. *Catal Lett* 53: 7-13
- Bumajdad A, Eastoe J, Zaki MI, Heenan RK, Pasupulety L (2007) Generation of metal oxide nanoparticles in optimised microemulsions. *J Colloid Interf Sci* 312: 68-75
- Cao S, Zhu Y (2008) Hierarchically nanostructured α -Fe₂O₃ hollow spheres: Preparation, growth mechanism, photocatalytic property, and application in water treatment. *J Phys Chem C* 112: 6253-6257
- Cao X, Prozorov R, Kolytyn Y, Kataby G, Felner I, Gedanken A (1997) Synthesis of pure amorphous Fe₂O₃. *J Mater Res* 12: 402-406
- Chauhan P, Annapoomi S, Trikha SK (1999) Humidity-sensing properties of nanocrystalline haematite thin films prepared by sol-gel processing. *Thin Solid Films* 346: 266-168
- Chunhui S, Mu P, Runzhang Y (2008) The effect of particle size gradation of conductive fillers on the conductivity and the flexural strength of composite bipolar plate. *Int J Hydrogen Energ* 33: 1035-1039
- Cornell RM, Giovanoli R (1985) Effect of solution conditions on the proportion and morphology of goethite formed from ferrihydrite. *Clay Clay Miner* 33: 424-432
- Cornell RM, Schwertmann U (1996) *The iron oxides: structure, properties, reaction, occurrences and uses*. Wiley-VCH, Weinheim

- Cornell RM, Schwertmann U (2003) The iron oxides: structure, properties, reaction, occurrences and uses. Wiley-VCH, Weinheim
- Diamandescu L, Mihaila-Tarabasanu D, Popescu-Pogrion N, Totovina A, Bibicu I (1999) Hydrothermal synthesis and characterization of some polycrystalline α -iron oxides. *Ceram Int* 25: 689-692
- Han L-H, Liu H, Wei Y (2011) In situ synthesis of hematite nanoparticles using a low-temperature microemulsion method. *Powder Technol* 207: 42-46
- Han MG, Armes SP (2003) Synthesis of poly(3,4-ethylenedioxythiophene)/silica colloidal nanocomposites. *Langmuir* 19: 4523-4526
- Hu X, Yu JC (2008) Continuous aspect-ratio tuning and fine shape control of monodisperse α -Fe₂O₃ nanocrystals by a programmed microwave-hydrothermal method. *Adv Funct Mater* 18: 880-887
- Huang Z, Feng Q, Chen Z, Chen S, Du Y (2003) Surface and size effects of magnetic properties in ferromagnetic nanoparticles. *Microelectron Eng* 66: 128-135
- Huo L, Li W, Lu L, Cui H, Xi S, Wang J, Zhao B, Shen Y, Lu Z (2000) Preparation, structure, and properties of three-dimensional ordered α -Fe₂O₃ nanoparticulate film. *Chem Mater* 12: 790-794
- Jing Z, Wu S (2004) Synthesis and characterization of monodisperse hematite nanoparticles modified by surfactants via hydrothermal approach. *Mater Lett* 58: 3637-3640
- Kandori K, Ohnishi S, Fukusumi M, Morisada Y (2008) Effects of anions on the morphology and structure of hematite particles produced from forced hydrolysis of Fe(NO₃)₃-HNO₃. *Colloid Surface A* 331: 232-238
- Kay A, Cesar I, Gratzel M (2006) New benchmark for water photooxidation by nanostructured α -Fe₂O₃ films. *J Am Chem Soc* 128: 15714-15721
- Li L, Li G, Smith RL Jr, Inomata H (2000) Microstructural evolution and magnetic properties of NiFe₂O₄ nanocrystals dispersed in amorphous silica. *Chem Mater* 12: 3705-3714
- Lian J, Duan X, Ma J, Peng P, Kim T, Zheng W (2009) Hematite (α -Fe₂O₃) with various morphologies: ionic liquid-assisted synthesis, formation mechanism, and properties. *ACS Nano* 3: 3749-3761.

- Lian S, Wang E, Kang Z, Bai Y, Gao L, Jiang M, Hu C, Xu L (2004) Synthesis of magnetite nanorods and porous hematite nanorods. *Solid State Commun* 129: 485-490
- Liu H, Ma M, Qin M, Yang L, Wei Y (2010) Studies on the controllable transformation of ferrihydrite. *J Solid State Chem* 183: 2045-2050
- Liu H, Wei Y, Sun Y (2005) The formation of hematite from ferrihydrite using Fe(II) as a catalyst. *J Mol Catal A-Chem* 226: 135-140
- Liu H, Wei Y, Li P, Zhang Y, Sun Y (2007) Catalytic synthesis of nanosized hematite particles in solution. *Mater Chem Phys* 102: 1-6
- Lu J, Chen D, Jiao X (2006) Fabrication, characterization, and formation mechanism of hollow spindle-like hematite via a solvothermal process. *J Colloid Interf Sci* 303: 437-443
- Min C, Huang Y, Liu L (2007) High-yield synthesis and magnetic property of hematite nanorhombos through a facile solution route. *Mater Lett* 61: 4756-4758
- Music S, Krehula S, Popovic S, Skoko Z (2003) Some factors influencing forced hydrolysis of FeCl₃ solutions. *Mater Lett* 57: 1096-1102
- Ocana M, Morales MP, Cerna CJ (1995) The growth mechanism of α -Fe₂O₃ ellipsoidal particles in solution. *J Colloid Interf Sci* 171: 85-91
- Petcharoen K, Sirivat A (2012) Synthesis and characterization of magnetite nanoparticles via the chemical co-precipitation method. *Mat Sci Eng B Solid* 177: 421-427
- Raming TP, Winnubst AJA, van Kats CM, Philipse AP (2002) The synthesis and magnetic properties of nanosized hematite (α -Fe₂O₃) particles. *J Colloid Interf Sci* 249: 346-350
- Ristic M, De Grave E, Music S, Popovic S, Orehovec Z (2007) Transformation of low crystalline ferrihydrite to α -Fe₂O₃ in the solid state. *J Mol Struct* 834: 454-460
- Sarangi PP, Vadera SR, Patra MK, Prakash C, Ghosh NN (2009) DC electrical resistivity and magnetic property of single-phase α -Fe₂O₃ nanopowder synthesized by a simple chemical method. *J Am Ceram Soc* 92: 2425-2428

- Schwertmann U, Friedl J, Stanjek H (1999) From Fe(III) ions to ferrihydrite and then to hematite. *J Colloid Interf Sci* 209: 215-223
- Su C, Wang H, Liu X (2011) Controllable fabrication and growth mechanism of hematite cubes. *Cryst Res Technol* 46: 209-214
- Sun Q, Lu X, Liang G (2010) Controlled template-free hydrothermal synthesis of hematite nanoplatelets. *Mater Lett* 64: 2006-2008
- Tang B, Wang G, Zhuo L, Ge J, Cui L (2006) Facile route to α -FeOOH and α -Fe₂O₃ nanorods and magnetic property of α -Fe₂O₃ nanorods. *Inorg Chem* 45: 5196-5200
- Teja AS, Koh P-Y (2009) Synthesis, properties, and applications of magnetic iron oxide nanoparticles. *Prog Cryst Growth Ch* 55: 22-45
- Vatta LL, Sanderson RD, Koch KR (2006) Magnetic nanoparticles: properties and potential applications. *Pure Appl Chem* 78: 1793-1801
- Wang D, Cao C, Xue S, Zhu H (2005) γ -Fe₂O₃ oriented growth by surfactant molecules in microemulsion. *J Cryst Growth* 277: 238-245
- Watanabe A, Kozuka H (2003) Photoanodic properties of sol-gel-derived Fe₂O₃ thin films containing dispersed gold and silver particles. *J Phys Chem B* 107: 12713-12720
- Wu Z, Yu K, Zhang S, Xie Y (2008) Hematite hollow spheres with a mesoporous shell: controlled synthesis and applications in gas sensor and lithium ion batteries. *J Phys Chem C* 112: 11307-11313
- Zhang YC, Tang JY, Hu XY (2008) Controllable synthesis and magnetic properties of pure hematite and maghemite nanocrystals from a molecular precursor. *J Alloy Compd* 462: 24-28
- Zysler RD, Mansilla M., Fiorani D (2004) Surface effects in α -Fe₂O₃ nanoparticles. *Eur Phys J B* 41: 171-175

Table Caption

Table 4.1 Summary of the magnetic parameters of the synthesized hematite nanoparticles with different particle sizes and morphologies

Figure Captions

Figure 4.1 XRD patterns of the 2-line ferrihydrite precursor ($C = 0.3$ M, pH 7) and the synthesized hematite nanoparticles ($C = 0.3$ M, $n_{\text{Fe(II)}}/n_{\text{Fe(III)}} = 0.02$, pH 7, 100 °C, and 1h).

Figure 4.2 FT-IR spectra of the 2-line ferrihydrite precursor ($C = 0.3$ M, pH 7) and the synthesized hematite nanoparticles ($C = 0.3$ M, $n_{\text{Fe(II)}}/n_{\text{Fe(III)}} = 0.02$, pH 7, 100 °C, and 1h).

Figure 4.3 TG-DTA curves of the synthesized hematite nanoparticles ($C = 0.3$ M, $n_{\text{Fe(II)}}/n_{\text{Fe(III)}} = 0.02$, pH 7, 100 °C, and 1h).

Figure 4.4 Average particle sizes of the synthesized hematite nanoparticles under the effect of various preparation conditions: (a) the precursor concentration; (b) the solution pH; (c) the amount of Fe(II); and (d) the ionic strength.

Figure 4.5 FE-SEM images of: (a) the 2-line ferrihydrite precursor ($C = 0.3$ M, pH 7); and the synthesized hematite nanoparticles ($n_{\text{Fe(II)}}/n_{\text{Fe(III)}} = 0.02$, pH 7, 100 °C, and 1h); (b) hematite $C = 0.1$ M; (c) hematite $C = 0.3$ M; and (d) hematite $C = 0.5$ M (Note: *inset plots* demonstrate the particle size distribution from the corresponding FE-SEM images).

Figure 4.6. FE-SEM images of the synthesized hematite nanoparticles with different morphologies: (a, b) the spherical-like particles at low and high magnifications; (c) the cubic-like particles; and (d) the ellipsoidal particles (Note: *inset* in (b) represents the magnified view of the particle surface).

Figure 4.7 Specific conductivities of the synthesized hematite nanoparticles with different particle sizes and morphologies.

Figure 4.8 Room temperature magnetization curves of the synthesized hematite nanoparticles with: (a) different particle sizes; and (b) different morphologies (Note: *dash line* is the same line as represented in (a); and *inset plots* illustrate the magnified view of the corresponding magnetization curves).

Table 4.1

Sample		Magnetic parameters			
Particle shape	Particle size (nm) ($\bar{X} \pm SD$)	H_c (Oe)	M_r (emu/g)	M_s (emu/g)	M_r/M_s
Sphere	49.3 \pm 8.8	30.2	0.00946	0.8018	0.01179
Sphere	91.7 \pm 15.1	115.3	0.17104	1.2874	0.13286
Sphere	139.5 \pm 28.2	211.5	0.56480	1.9433	0.29064
Cube	127.5 \pm 24.3	120.2	0.24456	1.7863	0.13691
Ellipsoid	119.4 \pm 44.3	185.2	0.31185	1.6332	0.19095

Note: H_c is the coercive force; M_r is the remanence magnetization (at $H = 0$ Oe); and M_s is the saturation (maximum) magnetization.

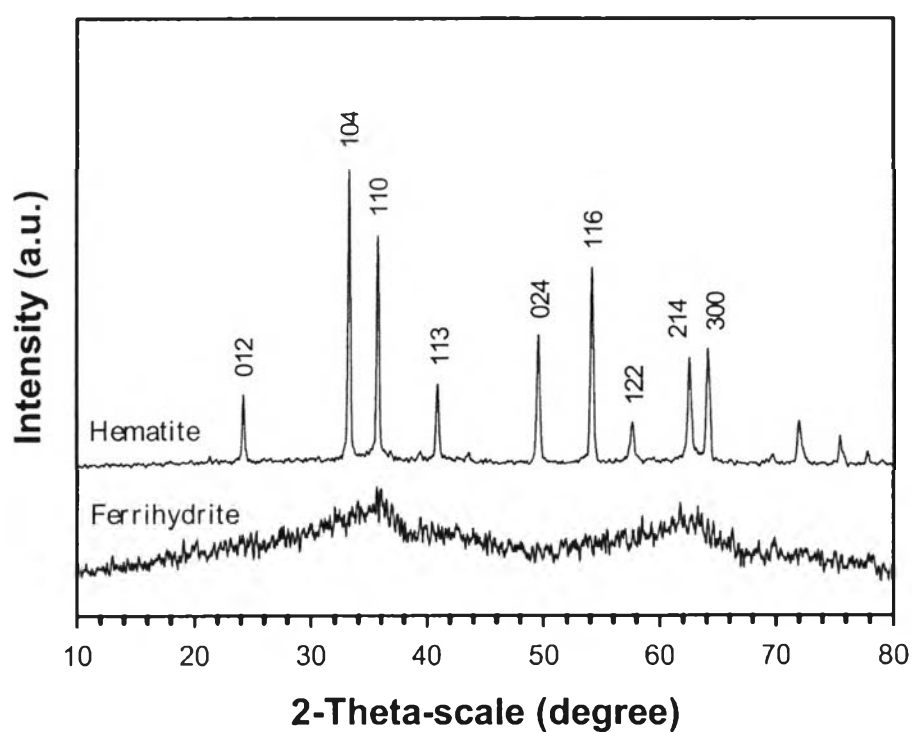


Figure 4.1

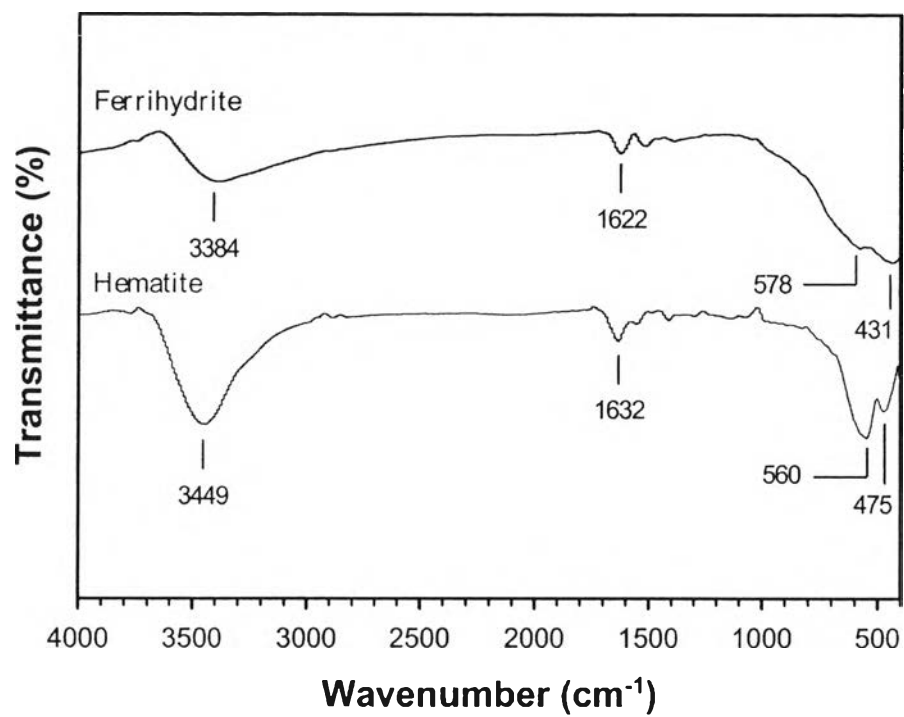


Figure 4.2

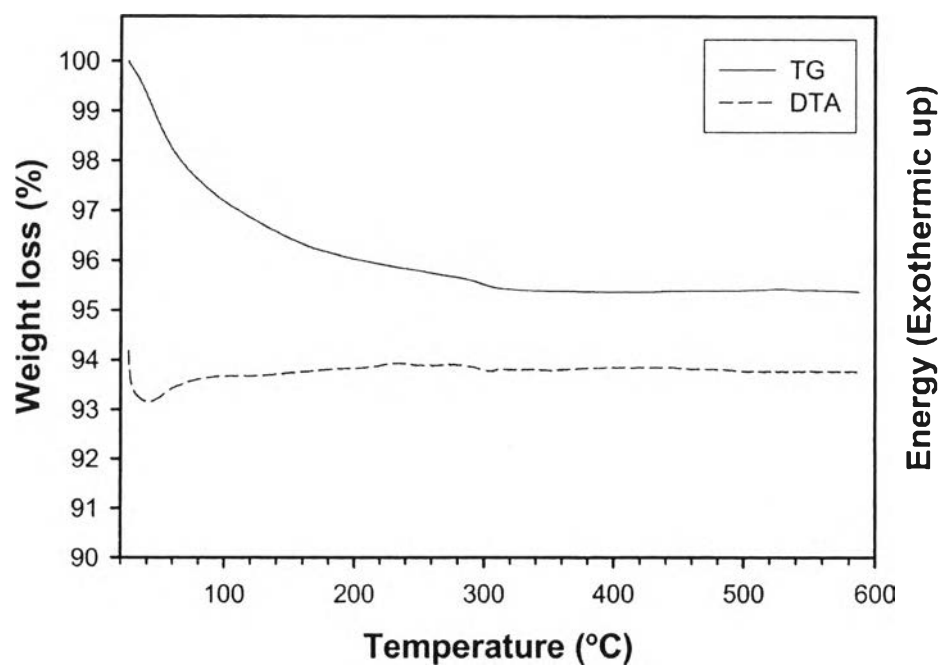


Figure 4.3

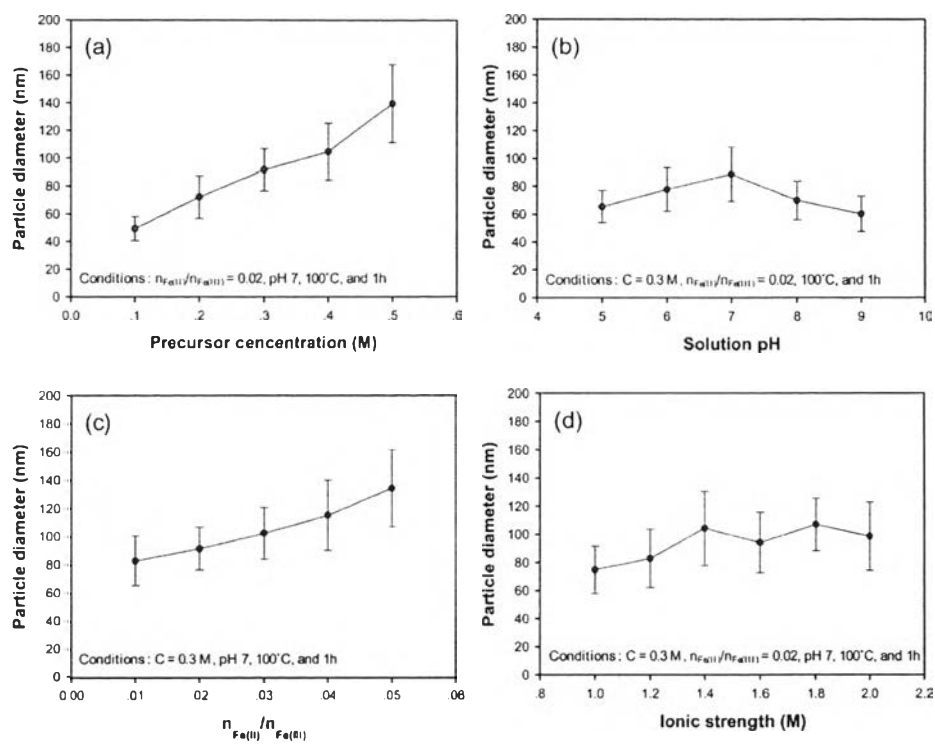


Figure 4.4

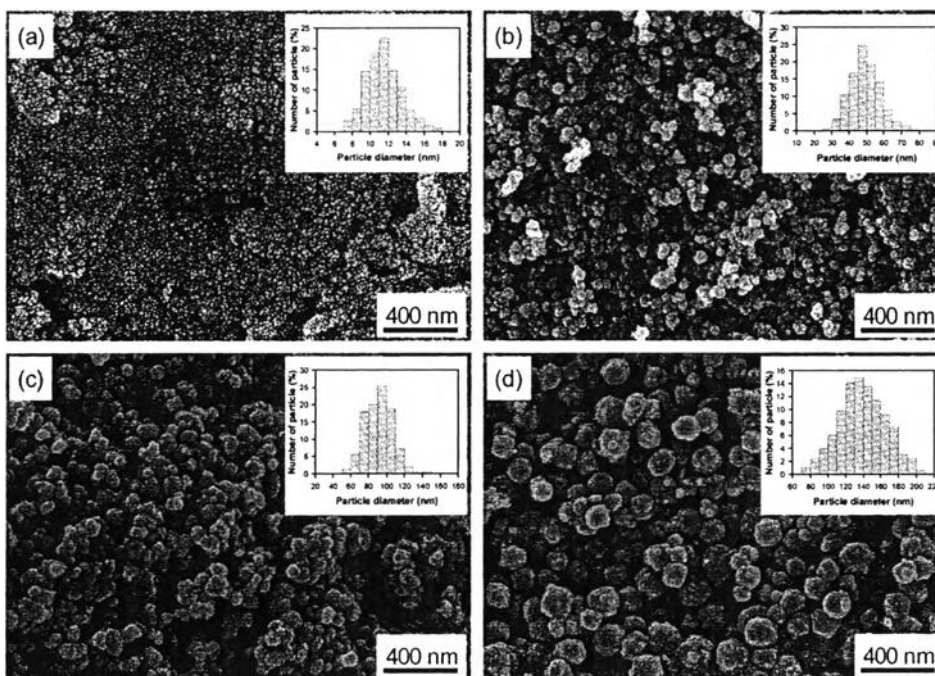


Figure 4.5

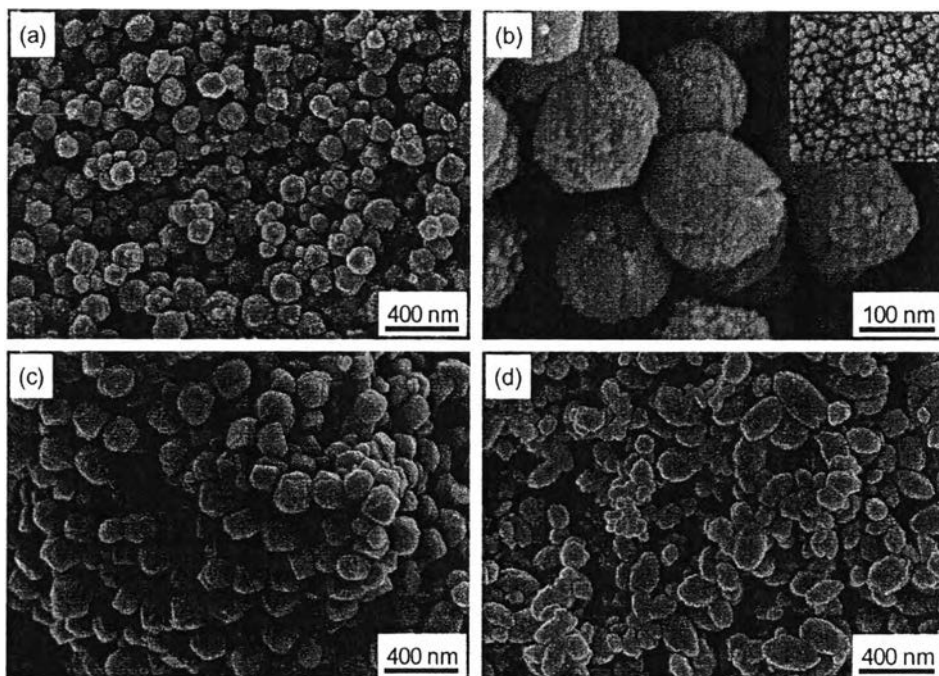


Figure 4.6

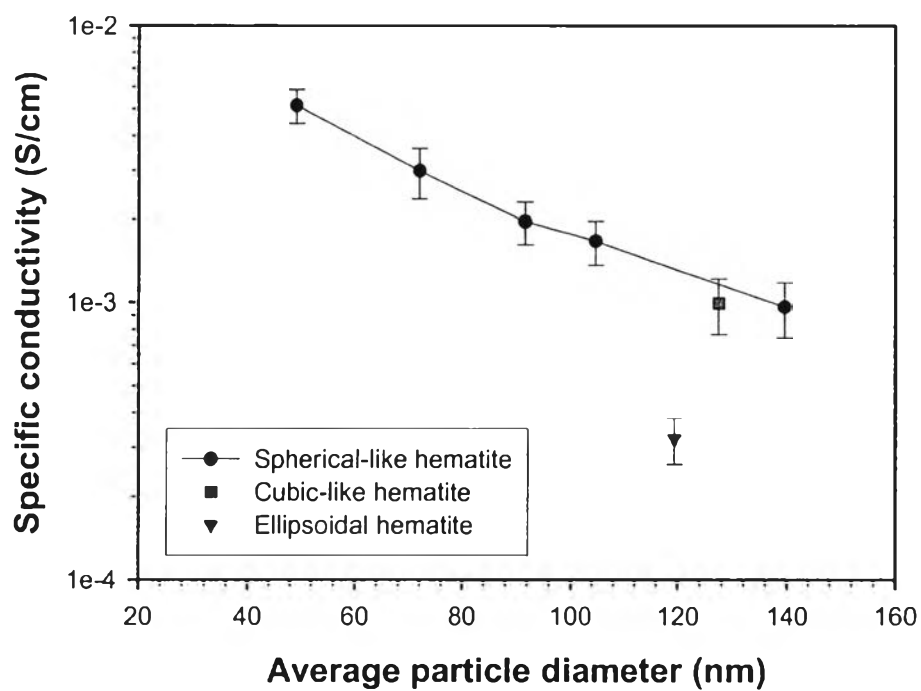


Figure 4.7

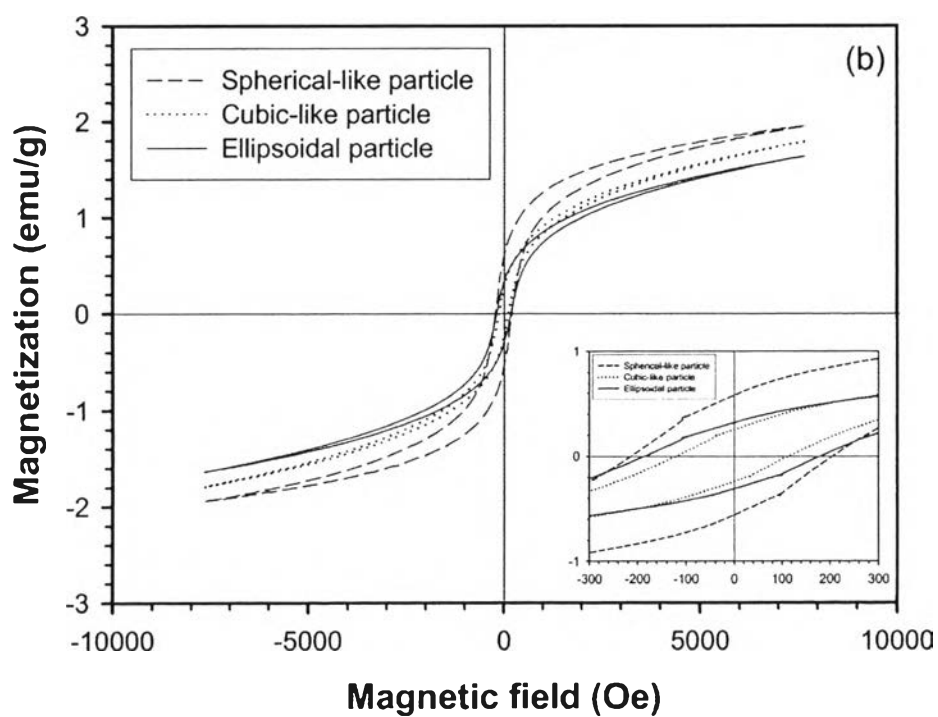
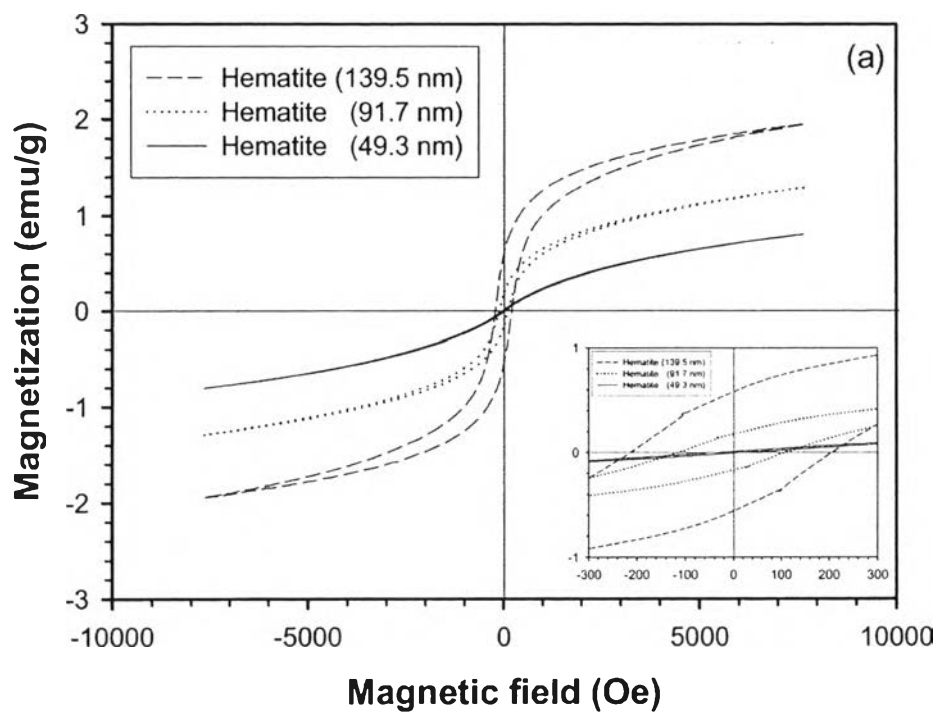


Figure 4.8